

Ballistic transport through coupled T-shaped quantum wires

Yuh-Kae Lin, Kao-Chin Lin and Der-San Chuu*

Department of Electrophysics, National Chiao Tung

University

1001 Ta Hsueh Road, Hsinchu, 30050 Taiwan

(today)

Abstract

The ballistic conductance of a coupled *T*-shaped semiconductor quantum wire (CTQW) are studied. Two types of CTQW are considered, one of which is a Π -shaped quantum wire (Π QW) which consists of two transverse wires on the same side of the main wire and the other a Π -clone quantum wire (Π CQW) which consists of two transverse wires on the opposite sides of the main wire. The mode matching method and Landauer-Buttiker theory are employed to study the energy dependence of the ballistic conductance. Most of transmission profiles of Π QW and Π CQW are found to be distinguishable for large separation d between the two transverse arms. The transmission probability manifests oscillatory behavior when d is increased. When a potential is added to the connection region, it results in decoupling or coupling effects between the two T-shaped wires according to whether it is positive or negative. When magnetic fields are applied to CTQW, the transmission profiles are found to be affected profoundly even if the electrons pass through

*Corresponding author email address: dschuu@cc.nctu.edu.tw; Fax:886-3-5725230; Tel:886-3-5712121-56105.

the field free region only.

71,23,An;71.24.+q;73.22.-f

I. INTRODUCTION

Recently, the microetching and epitaxial growth techniques have enabled semiconductor nanostructures to be fabricated with feature sizes down to nanometers. Such nanostructures include T-shaped quantum wires in which quasi-one-dimensional confinement is achieved at the intersection of two quantum wells. Both experimental and theoretical studies on the nonlocal ballistic transport of these structures have been stimulated. In general, T-shaped quantum wires can be fabricated by first growing a $\text{GaAs}/\text{Al}_x\text{Ga}_{1-x}\text{As}$ multilayers on a (001) substrate, after cleavage, a GaAs quantum well is grown over the exposed (110) surface, resulting in an array of T-shaped regions where carrier wavefunctions can be confined in several tens of angstroms. T-shaped quantum wires (TQW) possess some improved optical properties of one dimensional excitons, such as the excitonic laser emission, the enhancement of excitonic binding energy, and the concentrated oscillator strength. The conductance of such a mesoscopic structure exhibits many peculiar and interesting features due to its intrinsic nonlocality. Quantum conductance in mesoscopic structures is the consequence of a complex scattering process which involves the boundary and the shape of the potential across the structural geometry as a whole.

Several studies on the electronic transmission properties for a T-shaped quantum structure have been carried out.^{1–8} Many interesting transmission characteristics, such as resonant transmission and resonant reflection in the T- shaped structures have been revealed. Such behaviors are caused from the quantum interference which dominates the ballistic transport regime. Theoretically, one may view the resonance as being mediated by the quasibound states of the system. The system of T-shaped quantum wires has open geometry, therefore, the injected carriers that travel ballistically over the wire region will across the wire region and show a strong energy dependent transmission as a consequence of quantum interference effect induced by the interplay between the propagating modes of the wires.

By using the scattering matrix approach and Landauer-Buttiker theory, Goldoni *et. al.*⁴ have calculated the conductance of T-shape and coupled T-shaped quantum wires with dif-

ferent wire widths. The transmission coefficient of the whole coupled T-shaped quantum wires can be obtained easily since the total T-matrix is the product of the T-matrices of the isolated wires. The double resonance obtained in their result is ascribed to a fingerprint of the bonding and antibonding combinations of the resonance states of the isolated wires. Bohn⁵ has introduced a periodic array of T-shaped devices. He showed that deflected arrays exhibit a unique resonance structure with respect to electrons traveling along the array. The coefficients of the reflection and transmission through the array can peak simultaneously at resonance. Unlike the analogous case in superlattices, the peaks are at energies where the wavelength λ satisfies the condition $n\lambda/2 = d$ for some integer n . Consequently, the scattering wave function possesses nodes at the intersection of the longitudinal arm and the transversal arm, and thus greatly reduces the flux lost to transversal leads. Nikolic and Sordan⁶⁻⁷ have also studied the transmission properties of a quantum waveguide system with attached stubs in the ballistic regime. They found the transconductance and the differential drain conductance are small. Their result suggests limited abilities for conventional application of the transistor. Chen *et. al.*⁷ calculated transmission of electrons in a T-shaped opened quantum waveguide (TOQW) subjected to an inhomogeneous magnetic field perpendicular to the TOQW plane with mode-matching technique. The transmission profiles are found to depend sensitively on geometric parameters.

In this work, we study a II-shaped opened quantum structure and its clone shape, which are four-terminal waveguide-like structures, schematically as shown in Fig.1. We take first the geometric variation into account. Second, the interconnection region is considered to be acted by a potential. Third, the magnetic field is considered to apply to the vertical wires. Unlike the stubs, arms of the structures considered in our case are assumed to be long enough and open in the longitudinal and the transverse directions. The centers of the two vertical arms are spaced by a distance d as shown in Fig.1. The scattering matrice are calculated by using mode-mathing method. Our model will be presented briefly in the next section. Results and discussions will be given in the final section.

II. MODEL AND FORMALISM

We model the structure geometry as illustrated in Fig.1: A horizontal wire with a width of W_1 (W_2) for region I (VII), a vertical wire with a width of W_2 (W_3) for region II (V), an interconnection part for region IV and a junction region with an area of $W_1 \times W_2$ ($W_1 \times W_3$) for region III (VI). In the wire, 2DEG system with perfect barrier confinement (e.g. high quality interfaces) is assumed. The individual electron propagates ballistically through the entire wire. The transverse potential inside the wire is set to zero. The Schrödinger equation of individual electron can be written as

$$-\frac{\hbar^2}{2m} \nabla^2 \Psi = E \Psi \quad (1)$$

The whole quantum wire can be split into several individual homogeneous subregions: horizontal region I, vertical regions II and V, intersection region III and VI, interconnecting region IV, and the outgoing horizontal region VII. The two intersection regions act as scattering centers. And the interconnecting region acts as a connection of the two TQWs. An n th mode electron is considered to inject from left of region I into the wire. The wave function in region I can be written in terms of a sum of incident and reflecting modes as

$$\Psi_n^I(x, y) = \Phi_n^{I(+)}(y) e^{ik_n^{I(+)}(x+0.5W_2)} + \sum_m R_{mn} \Phi_m^{I(-)}(y) e^{ik_m^{I(-)}(x+0.5W_2)}, \quad (2)$$

where $k_n^{I(\pm)} = \sqrt{k^2 - (n\pi/W_1)^2}$, \pm represents the incident or reflecting mode, respectively, and $\Phi_n^{I(\pm)}$ are envelope functions in region I. The wave functions in regions II, V, and VII are given by a sum of outgoing modes respectively, i.e.,

$$\Psi_n^{II}(x, y) = \sum_m S_{mn}^{(1)} \Phi_m^{II(+)}(x) e^{ik_m^{II(+)}(y-0.5W_1)}, \quad (3)$$

$$\Psi_n^V(x, y) = \sum_m S_{mn}^{(2)} \Phi_m^{V(\pm)}(x) e^{ik_m^{V(\pm)}(y\mp0.5W_1)}, \quad (4)$$

where \pm represents the upward or downward arm and

$$\Psi_n^{VII}(x', y) = \sum_m T_{mn} \Phi_m^{VII(+)}(y) e^{ik_m^{VII(+)}(x'-0.5W_3)}. \quad (5)$$

The wave function in region IV is given by the sum of rightgoing (+) and leftgoing (−) modes,

$$\Psi_n^{IV}(x, y) = \sum_m \left[U_{mn} \Phi_m^{IV(+)}(y) e^{ik_m^{IV(+)}(x-0.5W_2)} + V_{mn} \Phi_m^{IV(-)}(y) e^{ik_m^{IV(-)}(x-0.5W_2)} \right]. \quad (6)$$

In region III and region VI, all modes must be taken into account, thus

$$\begin{aligned} \Psi_n^{III}(x, y) &= \sum_j f_j(y) \cdot \left[a_{jn} \sin(k'_j(x - 0.5W_2)) + b_{jn} \sin(k'_j(x + 0.5W_2)) \right] \\ &\quad + \sum_j g_j(x) c_{jn} \sin(k''_j(y + 0.5W_1)), \end{aligned} \quad (7)$$

$$\begin{aligned} \Psi_n^{VI}(x', y) &= \sum_j f_j(y) \cdot \left[d_{jn} \sin(k'_j(x' - 0.5W_3)) + e_{jn} \sin(k'_j(x' + 0.5W_3)) \right] \\ &\quad + \sum_j g'_j(x') h_{jn} \sin(k'''_j(y \pm 0.5W_1)). \end{aligned} \quad (8)$$

Here $f_j(y) = \sqrt{\frac{2}{W_1}} \sin\left(\frac{j\pi}{W_1}(y + 0.5W_1)\right)$, $g_j(x) = \sqrt{\frac{2}{W_2}} \sin\left(\frac{j\pi}{W_2}(x + 0.5W_2)\right)$ and $g'_j(x') = \sqrt{\frac{2}{W_3}} \sin\left(\frac{j\pi}{W_3}(x' + 0.5W_3)\right)$ represent the transverse wave functions of the electron in mode j inside the different regions of the wires, and are used as the expansion bases. The wave numbers $k'_j = \sqrt{k^2 - (j\pi/W_1)^2}$, $k''_j = \sqrt{k^2 - (j\pi/W_2)^2}$, and $k'''_j = \sqrt{k^2 - (j\pi/W_3)^2}$ are either real for propagating modes or pure imaginary for evanescent modes. Now expand the wavefunctions in terms of a set of complete bases corresponding to the transverse eigenfunctions in regions I, II, IV, V and VII, respectively as

$$\Phi_n^{I(\pm)}(y) = \sum_j \alpha_{jn}^{I(\pm)} f_j(y), \quad (9)$$

$$\Phi_n^{II(+)}(x) = \sum_j \beta_{jn}^{II(+)} g_j(x), \quad (10)$$

$$\Phi_m^{IV(\pm)}(y) = \sum_j \gamma_{jm}^{IV(\pm)} f_j(y), \quad (11)$$

$$\Phi_n^{V(\pm)}(x') = \sum_j \delta_{jn}^{V(\pm)} g'_j(x'), \quad (12)$$

and

$$\Phi_n^{VII(+)}(y) = \zeta_{jn}^{VII(+)} f_j(y). \quad (13)$$

Substituting these functions into Eq.(1) for a given Fermi energy E_F , we obtain five sets of eigen-wave-numbers $\{k_n^{I(\pm)}\}$, $\{k_n^{II(+)}\}$, $\{k_n^{IV(\pm)}\}$, $\{k_n^{V(\pm)}\}$, and $\{k_n^{VII(+)}\}$ and eigen-wave-functions $\{\Phi_n^{I(\pm)}(y)\}$, $\{\Phi_n^{II(+)}(y)\}$, $\{\Phi_n^{IV(\pm)}(y)\}$, $\{\Phi_n^{V(\pm)}(y)\}$, and $\{\Phi_n^{VII(+)}(x)\}$. By using boundary matching technique,⁹ we can derive all coefficients in Eqs. (2)–(8) such as $\{r_{mn}\}$, $\{s_{mn}^{(1)}\}$, $\{s_{mn}^{(2)}\}$, $\{u_{mn}\}$, $\{v_{mn}\}$, $\{t_{mn}\}$, $\{a_{jn}\}$, $\{b_{jn}\}$, $\{c_{jn}\}$, $\{d_{jn}\}$, $\{e_{jn}\}$, and $\{h_{jn}\}$.

The group velocities of the j th state in region I, II, V and VII are respectively

$$V_j^{I(\pm)} = \frac{\hbar}{m^*} \int_{-0.5W_1}^{0.5W_1} \Phi_j^{I(\pm)}(y) k_j^{I(\pm)} \Phi_j^{I(\pm)}(y) dy, \quad (14)$$

$$V_j^{II(+)} = \frac{\hbar}{m^*} \int_{-0.5W_2}^{0.5W_2} \Phi_j^{II(+)}(x) k_j^{II(+)} \Phi_j^{II(+)}(x) dx, \quad (15)$$

$$V_j^{V(\pm)} = \frac{\hbar}{m^*} \int_{-0.5W_3}^{0.5W_3} \Phi_j^{V(\pm)}(x) k_j^{V(\pm)} \Phi_j^{V(\pm)}(x) dx, \quad (16)$$

as well as

$$V_j^{VII(+)} = \frac{\hbar}{m^*} \int_{-0.5W_1}^{0.5W_1} \Phi_j^{VII(+)}(y) k_j^{VII(+)} \Phi_j^{VII(+)}(y) dy. \quad (17)$$

The transmission probabilities \tilde{t}_{nj} (in region VII) and $\tilde{s}_{nj}^{(1)} \left(\tilde{s}_{nj}^{(2)} \right)$ (in region II and region V) from the incident mode n to the final mode j , and the reflection probability \tilde{r}_{nj} from the incident mode n to the final mode j (in region I) can be obtained, respectively, as follows:

$$\tilde{r}_{nj} = \frac{V_j^{I(-)}}{V_n^{I(+)}} |r_{nj}|^2, \quad (18)$$

$$\tilde{s}_{nj}^{(1)} = \frac{V_j^{III(+)}}{V_n^{I(+)}} |s_{nj}^{(1)}|^2, \quad (19)$$

$$\tilde{s}_{nj}^{(2)} = \frac{V_j^{III(+)}}{V_n^{I(+)}} |s_{nj}^{(2)}|^2, \quad (20)$$

$$\tilde{t}_{nj} = \frac{V_j^{II(+)}}{V_n^{I(+)}} |t_{nj}|^2. \quad (21)$$

It should be emphasized that the expansions (9)–(13) involve an infinite sum including all possible evanescent modes. In practice, in order to solve this set of equations numerically, we have to truncate the sum at some finite number which should be large enough to achieve a desired accuracy. The numerical convergence can be checked by flux conservation. The relationship $\sum_j (\tilde{t}_{jn} + \tilde{r}_{jn} + \tilde{s}_{jn}) = 1$ should be fulfilled accurately.

The total transmission coefficients T and S are then given by

$$T = \sum_{n=1}^{N_1} \sum_{j=1}^{N_2} \tilde{t}_{nj}, \quad (22)$$

$$S = \sum_{n=1}^{N_1} \sum_{j=1}^{N_3} \tilde{s}_{nj}. \quad (23)$$

Where N_1 , N_2 and N_3 are the numbers of propagating modes in regions I, II and III, respectively. The conductance G at zero temperature is given by the Landauer–Buttiker formula:

$$G_t = (2e^2/h)T \quad (24)$$

and

$$G_s = (2e^2/h)S. \quad (25)$$

We also evaluate the probability density of electrons in the quantum wire by adding the contributions from all propagating modes as

$$\rho(x, y) = \sum_{n=1}^N |\Psi_n(x, y)|^2 / k_n. \quad (26)$$

III. NUMERICAL RESULTS AND DISCUSSIONS

A. Transmission Properties with Geometric Variations

Figs.1(a) and (b) schematically depict the geometry of the Π –shaped QW (Π QW) and the Π –clone QW (Π CQW). We present our results in terms of some convenient parameters:

1) the first threshold energy $E_1 = \frac{\hbar^2}{2m^*}(\pi/W_1)^2$ through horizontal wire, 2) the distance d between two center of the intersections of vertical wires and horizontal wire, 3) the ratios of widths $\alpha = W_2/W_1$ and $\gamma = W_3/W_2$.

First of all, we consider that all wires are the same width, namely W . Transmission probabilities are calculated with varying k_F as shown in Fig. 2(a) and (b) for different d . Curves from bottom to top in Fig.2(a) are shifted by 1.0 for clarity and correspond to the cases of $d = 1, 1.1, 1.2, 1.3, 1.5, 1.7$, and $2.0W_1$, respectively. And curves from bottom to top in Fig.2(b) are shifted by 1.0 for clarity and correspond to the cases of $d = 2, 2.5, 3.0$, and $5.0W_1$, respectively. Hereafter, we present the transmission probabilities of the Π QW system as solid lines and those of the Π CQW system as the dotted lines in all figures.

For $d = 1$, the vertical wires are adjacent to each other. Thus, a Π QW with $d = 1$, can be regarded as a TQW with a double width in the vertical arm except there is an infinite thin wall along the vertical arm axis. However, one can note from the figure that the profiles of transmission of a Π QW with $d = 1$ are quite different from the transmission profiles of a TQW with the same width ($2.0W_1$) of the vertical arm⁸. In fact, the bottom curve of Π QW ($d = 1$) is similar to the result obtained in TQW with a vertical arm of $1.0W_1$ width as obtained in Ref (8). This implies that the two systems are similar except the transmission amplitude is suppressed in a Π QW system. For the Π CQW, the sharp dip at $k_F = 2.0\pi/W_1$ is replaced by a wider valley before $k_F = 2.0\pi/W_1$. The transmission behaviors of the two structures (Π QW and Π CQW) are different in general, however, their periodic oscillations are the same. The period of the oscillation is dominated by the distance d as can be seen from Fig.2. The periodicity can be fitted as $n\lambda_l = 2d$ approximately, where n is the number of periods in one mode, and $\lambda_l = 2\pi/(k_F - \pi/W_1)$ denotes the longitudinal wave length of the incident electron waves. Thus, once one finds two peaks in the region $1.0 < k_FW_1/\pi < 2.0$ for $d = 1W_1$, then four peaks will be found for $d = 2W_1$, and so on. Curves in both structures (Π QW and Π CQW) possess peak-dip structures. Especially, these peak-dip structures are more clear for larger d at $k_F = 2.0\pi/W_1$. On the contrary,

they are observed only in certain circumstance for smaller d . According to the previous result⁸, there exists a localized state in the intersection region for a symmetric TOQW with same wavenumber $k_F = 2.0\pi/W_1$. The peak-dip structure at $k_F = 2.0\pi/W_1$ can be ascribed to this localized state. The peak-dip structure is found at $k_F = 2.0\pi/W_1$ on the curve with $d = 1.5$ for Π CQW. For d larger than $1.5W_1$, the peak-dip structure is sharper in Π CQW than that in Π QW.

Due to the fact that both Π QW and Π CQW structures are equivalent to a system of two TQWs, one may expect that the transmission properties of these two structures will be the same if the coupling between the constituent TQWs becomes very weak. However, our result does not manifest this accordance. On the contrary, the two transmission profiles are still distinguishable from each other even for large d . It is also found that the transmission probabilities vary periodically with d for a fixed wavenumber as shown in Fig.3. These behaviors are the essential characteristics of ballistic theory.

Now let us consider the case that the widths of the vertical wires are the same, while the ratio of the width of the vertical wire to the horizontal wire is varied. The result is displayed in Fig. 4. For simplicity, we define the ratio of the width of the vertical wire to the horizontal wire as $\alpha = W_2/W_1 = W_3/W_1$. And the distance d is set to $2\alpha W_1$. Curves from the bottom to the top are shifted by 1.0 individually for clarity and correspond to the cases of $\alpha = 0.1, 0.2, 0.3, 0.5, 0.7, 1.0, 1.5, 2.0$ and 4.0 , respectively, as shown in the figure. For extremely small α , perfect stepwise profiles are observed in both structures. The transmissions are strongly suppressed when the ratio α is large (e.g. 2.0 and 4.0). The solid curve for $\alpha = 0.5$ agrees with the result of previous work⁴. A double resonance is evident either on the curve of $\alpha = 0.3$ or the curve of $\alpha = 0.5$. They are the signature of the bonding and antibonding combinations of the resonant quasi-1D state of isolated wires.

Finally, the transmission profiles in the Π QW and Π CQW with vertical wires of different width are considered. For simplicity, the width of one vertical wire is kept to be the same as that of the horizontal wire. The calculated transmission profiles for $W_1 = W_3$ and different W_2 are shown in Fig.5(a) and those for $W_1 = W_2$ and various W_3 are shown in Fig.5(b).

Curves are offset for clarity. Curves from bottom to top correspond to the cases of $\alpha=0.1, 0.2, 0.3, 0.5, 0.7, 1.0, 2.0, 4.0$, and 5.0 , respectively. Where α is the ratio of the wire width of the vertical wire to the horizontal wire. It is observed that the transmission probability is drastically suppressed for large α as can be seen from the upper curves in (a) and (b). Comparing curves in (a) and (b), we observe that the transmission profiles are the same. When α is small, the transmission profiles of the Π QW and Π CQW become indistinguishable and almost the same as that of TQW system. The double resonance can be observed again.

B. Transmission Under an Additional Potential

We now consider the case that an additional scalar potential is applied to the interconnection region IV. The applied potential can be negative or positive for attracting or depleting electrons. The different coupling profiles are interesting and may be important for practical usage of the mesoscopic devices.

Fig.6 presents the calculated transmission profiles for different potential strength V_4 in unit of E_1 . Here we consider $W_3 = W_2 = W_1$, and $d = 2W_1$. Figs.6(a) and (c) correspond to the positive potential for electrons. Figs.6(b) and (d) correspond to negative potential. Curves are offset for clarity. As shown in Fig.6(a), one can observe that the positive potential does not affect the transmission very much when $V_4 \leq E_1$. From Figs.6(a) and (c), two features are shown: (1) the onset is shifted due to the depletion potential; (2) the positions of transmission dips are not changed. On the contrary, Figs.6(b) and (d) show that the additional negative potential affects the transmission much stronger than the positive one. Especially, the potential enhances the coupling between the two TOQWs as one can note from the fact that the resonant dip-peak-dip structure becomes broader and shallower when the potential is increased. More peaks are on the curves and the positions of dips are not changed as the case of positive potential. Moreover, it can be observed that discrepancy between the two structures becomes prominent as the potential strength is increased. These results manifest that the negative potential increases the coupling strength between the two

individual TOQWs.

C. Transmissions under the influence of surrounding magnetic Fields

Finally, magnetic fields are considered to apply to the vertical wires only, therefore, the electrons pass through the main arm regions with no additional field. We shall study the effect of the surrounding magnetic fields on the transmission behavior. First, we consider the magnetic field is applied only to one of the vertical wires, i.e on arm II or arm V. The direction of the field is perpendicular to the 2DEG plane. Transmission probabilities are calculated as a function of Fermi wave vector as depicted in Fig.7. Curves in Fig.7(a) are offset for clarity, and correspond to the cases of magnetic field strength $B = -1.0, -0.7, -0.5, -0.3, -0.2, -0.1, 0.1, 0.2, 0.3, 0.5, 0.7, 1.0$ Tesla, respectively in region II. Those shown in Fig.7(b) are the same except the magnetic field is applied to region V. From these curves, one can conclude that: (1) the magnetic field does affect the transmission, although the electrons do not pass through the region with magnetic field directly. This phenomenon is according with Aharonov-Bohm effect. However, no periodic behavior can be found. (2) For the Π QW system as shown in solid curves in Figs.7(a) and (b), both cases show a one-to-one correspondence to each other. This manifests that the influence of the magnetic field on the transmission profile depends only on the magnetic field strength. However, there is no correspondence in the case of Π CQW which is presented by the dotted lines in Figs.7(a) and (b). (3) Generally speaking, opposite polarity of the magnetic field causes different influence on the transmission in Π CQW systems.

The transmission profiles versus Fermi wave number k_F for the case that the magnetic field being applied to both regions II and V, are displayed in Fig.8. Fig.8(a) presents the transmission in the Π QWs and Π CQWs with same polarity in both vertical arms, and Fig.8(b) presents those with opposite polarity to each other in the two vertical arms. The curves are offset for clarity. The solid lines represent the Π QW systems and dotted lines represent the Π CQW systems. It is found that for the case of Π QWs, though the geometry

and the applied field are symmetric, the transmission probabilities are different from each other (e.g. the solid curves with $v = 0.2$ and -0.2) as can be seen from Fig.8(a). However, for the case of Π CQWs, the transmission are polarity independent as can be noted from the dotted curves in Fig.8(a). No such symmetry can be found in Π CQW as shown in Fig.8(b). Furthermore, peak-dip structures are evident both in Figs.(a) and (b) at high field situations, though the electrons always move in field free region. One can expect that the transmission profiles will become stepwise structures when the applied magnetic field is extremely high. And in the intermediate field strength, the magnetic field changes the oscillatory behavior of the profiles significantly.

IV. SUMMARY

In the present work, the transmission properties of the coupled TOQWs are found to be very sensitive to the geometric configurations as well as the strength and polarity of the applied fields. A double resonance is observed on the profiles at certain ratio of the width of the vertical wire to the horizontal wire. The transmission is suppressed drastically as the width of one or both vertical wires become large. Most of the transmission profiles of Π QW and Π CQW are distinguishable even for large inter- distance d between the two vertical wires. The transmission profiles exhibit oscillatory behavior as the distance d is increased and manifest periodic features as the distance d is varied. T-shaped quantum wires have been proposed to achieve the quantum interference effect by controlling the length of its lateral closed arms. In the present study, it is found that the interference pattern can be easier to obtain by modulating the length and width of transversal arms and the distance between arms.

When a potential is added to the connection region, it results in decoupling or coupling effects between the two TQWs according to whether it is positive or negative. This behavior is observed by the alternating occurrence of the successive dips and valleys when the potential is increased positively.

Though the electrons pass through only the field free region, the magnetic field still affects the transmission in the QWs profoundly. The perfect transmission can be seen only in the high magnetic field region.

Acknowledgement: This work is supported partially by National Science Council, Taiwan under the grant number NSC91-2112-M-009-002.

REFERENCES

- [1] F. Sols, M. Macucci, U. Ravaili, and K. Hess, *J. Appl. Phys.* **66**, 3892 (1989); F. Sols and M. Macucci, *Phys. Rev. B* **41**, 11887 (1990).
- [2] J. Wang and H. Guo, *Appl. Phys. Lett.* **60**, 654 (1992).
- [3] R. Sordan and K. Nikolic, *Appl. Phys. Lett.* **68**, 3599 (1996).
- [4] G. Goldoni, F. Rossi, and E. Molinari, *Appl. Phys. Lett.* **71**, 1519 (1997).
- [5] J. L. Bohn, *Phys. Rev. B* **56**, 4132 (1997).
- [6] K. Nikolic and R. Sordan, *Phys. Rev. B* **58**, 9631 (1998).
- [7] B. -Y. Gu, Y. K. Lin, and D. S. Chuu, *J. Appl. Phys.* **86**, 1013 (1999); K.-Q. Chen, B.-Y. Gu, Y. K. Lin, and D. S. Chuu, *Intl. J. Mod. Phys. B* **13**, 903 (1999)
- [8] Y. K. Lin, Y. N. Chen, and D. S. Chuu, *Phys. Rev. B* **64**, 193316 (2001); *J. Appl. Phys.* **91**, 3054 (2002).
- [9] J. Goldstone and R. L. Jaffe, *Phys. Rev. B* **45**, 14100 (1992).

FIGURES

FIG. 1. (a) The schematic illustrations of the geometries of a Π QW system. (b) a Π CQW system.

FIG. 2. The transmission T versus K_F for different d which is converted to v by $d = (1+v)W_1$. All wires have same width. (a) $d \leq 2W_1$ (b) $d \geq 2W_1$. The solid lines represent the T of Π QW, while the dotted lines represent the T of Π CQW.

FIG. 3. The periodic behaviors of transmissions versus d for $W_3 = W_2 = W_1$. $T_1(T_2), S_1(S_2)$ represent the total transmission coefficients T and S as defined in Eqs.(22) and (23) for Π QW (Π CQW).

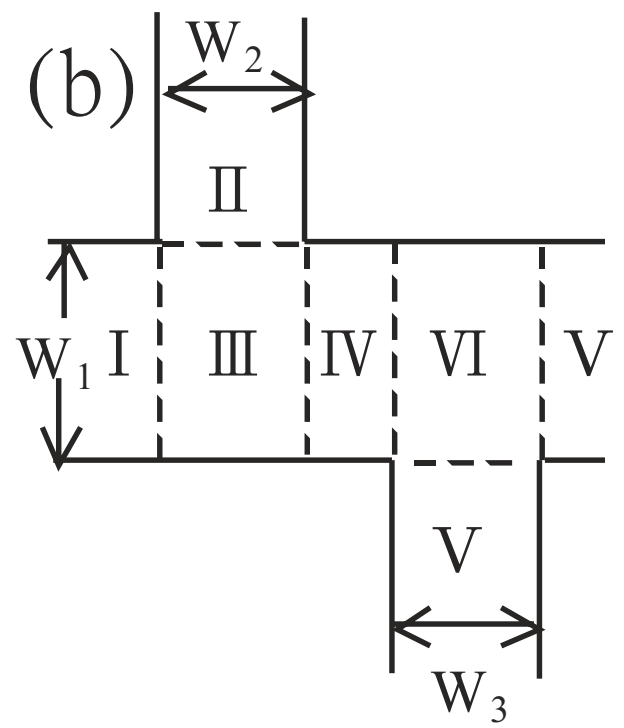
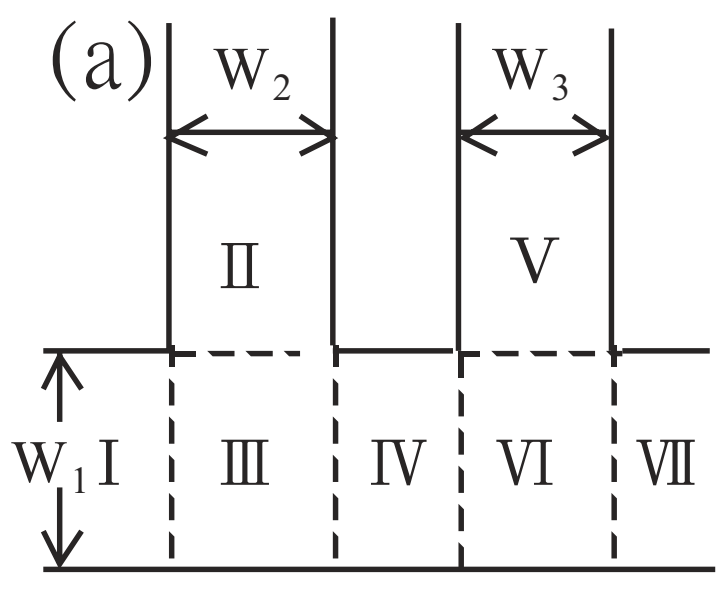
FIG. 4. Transmission versus k_F for different α . Where α is the ratio of the width of the vertical arm to the horizontal arm. And $d = 2\alpha W_1$. The solid lines represent the T of Π QW, while the dotted lines represent the T of Π CQW. Curves are offset for clarity.

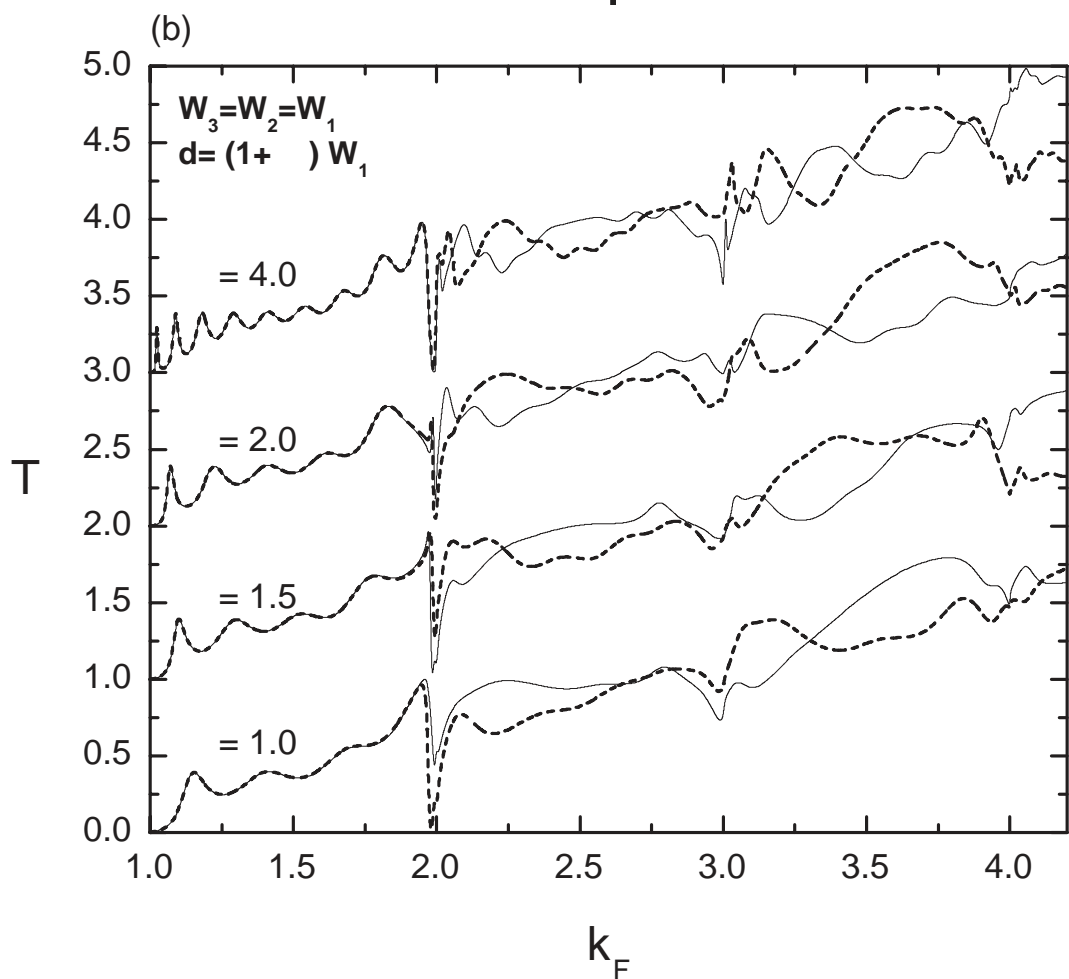
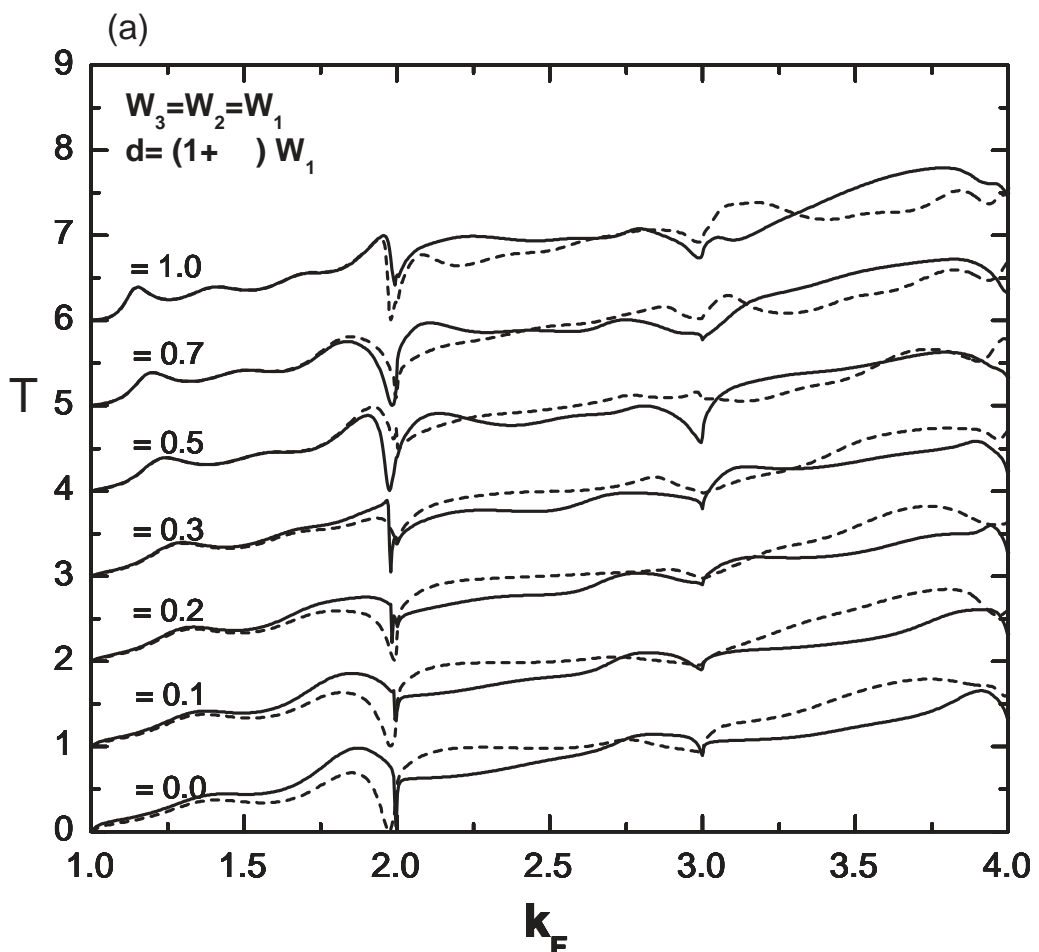
FIG. 5. Same as Fig.2, except the width of one vertical arm varies. (a) The width of W_2 varies, (b) the width of W_3 varies. The solid lines represent the T of Π QW, while the dotted lines represent the T of Π CQW.

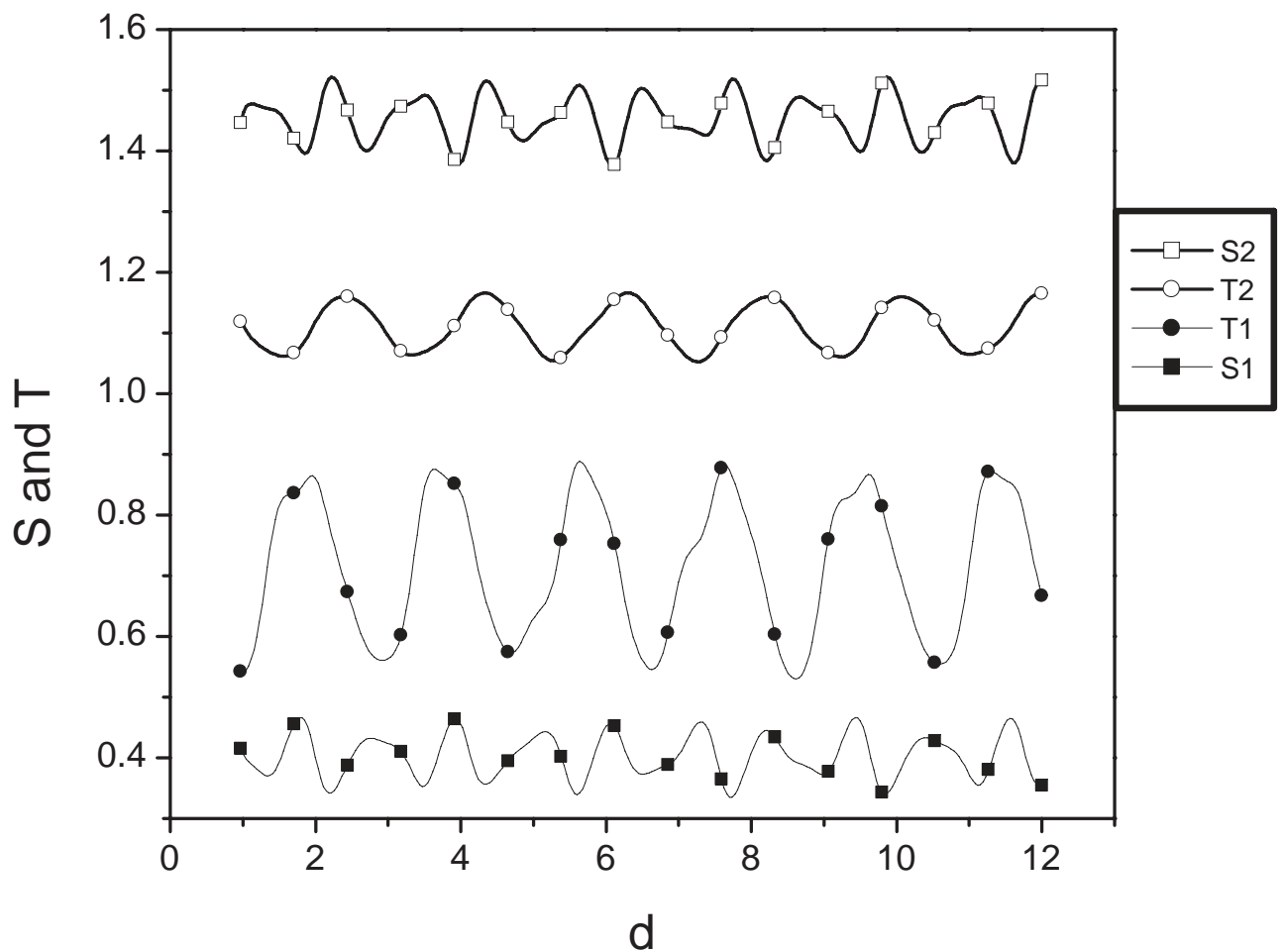
FIG. 6. Transmission profiles versus k_F for a potential V_4 applied to the region IV. (a) and (c) correspond to the positive potential and (b) and (d) correspond to the negative potential. The solid lines represent the T of Π QW, while the dotted lines represent the T of Π CQW.

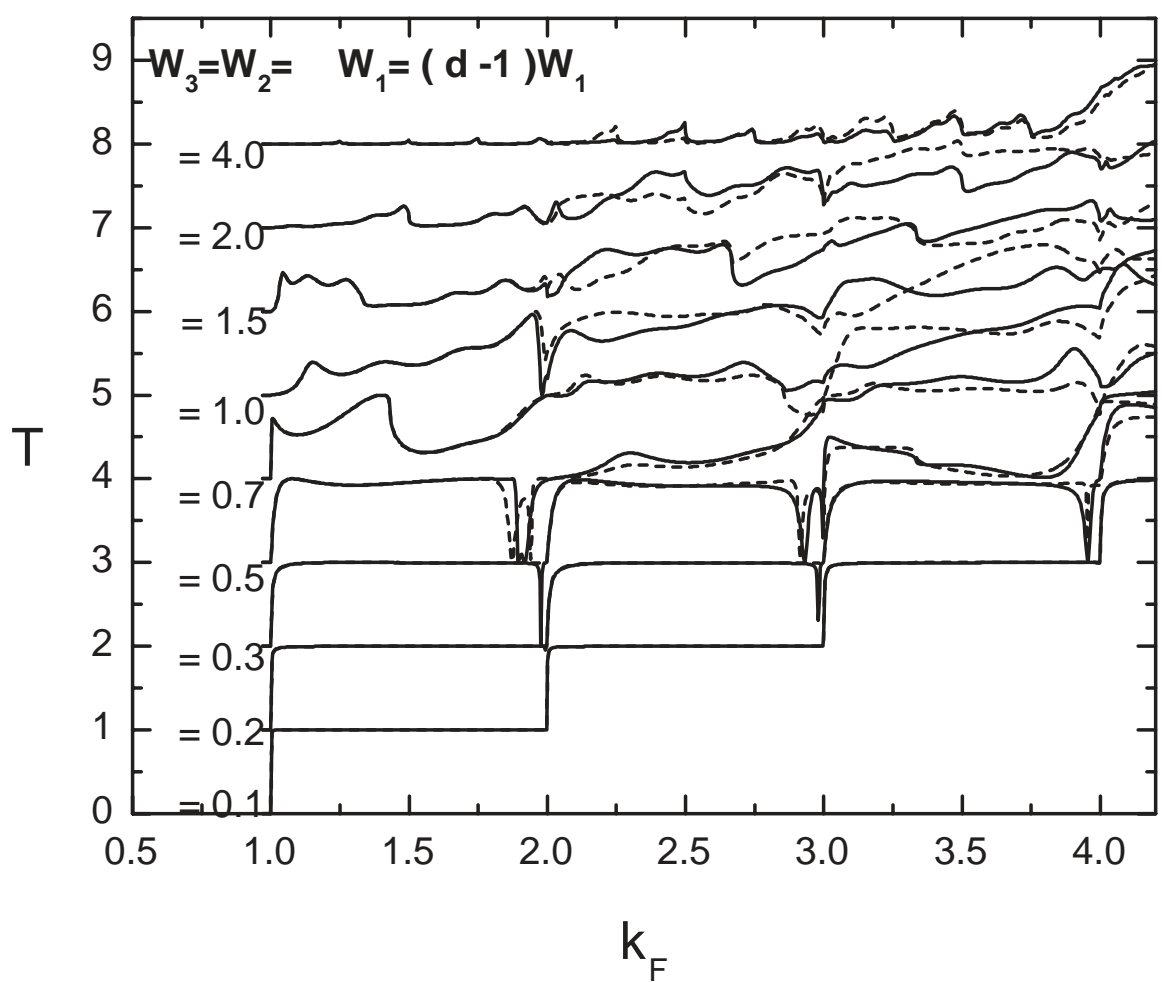
FIG. 7. Transmission profiles versus k_F for the magnetic field applied to only one vertical arm. (a) to region II, and (b) to region V. The solid lines represent the T of Π QW, while the dotted lines represent the T of Π CQW. Curves are offset for clarity.

FIG. 8. Transmission profiles versus k_F for the magnetic field applied to both vertical arms. (a) same polarity, and (b) opposite polarity in II and V. The solid lines represent the T of Π QW, while the dotted lines represent the T of Π CQW. Curves are offset for clarity.

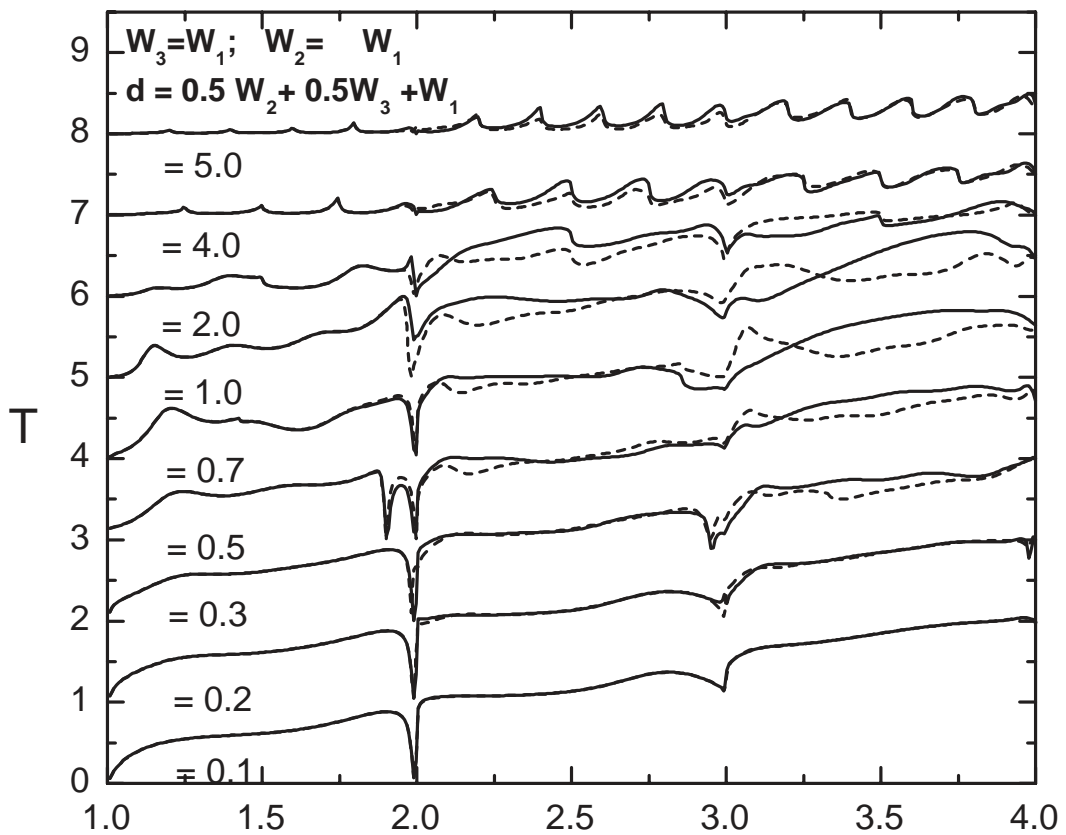








(a)



(b)

